Research Square

Preprints are preliminary reports that have not undergone peer review.
They should not be considered conclusive, used to inform clinical practice,
or referenced by the media as validated information.

Using aviation fuel hydrogen content to assess contrails and climate impact

Ziming Wang

ziming.wang@dlr.de

German Aerospace Center (DLR), Institute of Atmospheric Physics https://orcid.org/0000-0002-0219-1838

Christiane Voigt

DLR Deutsches Zentrum für Luft- und Raumfahrt https://orcid.org/0000-0001-8925-7731

Andreas Marsing

German Aerospace Center (DLR), Institute of Atmospheric Physics

Audrey Lecouffe

Sorbonne Université / CNRS, Institute Pierre-Simon Laplace

Marlin Juchem

German Aerospace Center (DLR), Institute of Atmospheric Physics https://orcid.org/0009-0000-0356-394X

Greg Smallwood

National Research Council Canada https://orcid.org/0000-0002-6602-1926

Simon Kirschler

German Aerospace Center https://orcid.org/0000-0003-4232-8277

Dennis Piontek

German Aerospace Center

Georg Eckel

DLR - German Aerospace Center https://orcid.org/0000-0002-6922-8279

Rebecca Dischl

German Aerospace Center (DLR), Institute of Atmospheric Physics

Raphael Märkl

German Aerospace Center (DLR), Institute of Atmospheric Physics

Daniel Sauer

DLR https://orcid.org/0000-0002-0317-5063

Ulrich Schumann

DLR https://orcid.org/0000-0001-5255-6869

Kai Widmaier

German Aerospace Center

Roger Teoh

Centre for Transport Studies, Department of Civil and Environmental Engineering, Imperial College London

Marc Stettler
Imperial College London https://orcid.org/0000-0002-2066-9380

Bastian Rauch
European Union Aviation Safety Agency (EASA)

Nicolas Bellouin
University of Reading, Department of Meteorology

Article

Keywords:

Posted Date: August 12th, 2026

DOI: https://doi.org/10.21203/rs.3.rs-10602102/v1

License: This work is licensed under a Creative Commons Attribution 4.0 International License.
Read Full License

Additional Declarations: There is **NO** Competing Interest.

Using aviation fuel hydrogen content to assess contrails and climate impact

Ziming Wang[1,2,3,*], Christiane Voigt[1,2], Andreas Marsing[1], Audrey Lecouffe[3], Marlin Juchem[1,2], Greg Smallwood[4,5], Simon Kirschler[1], Dennis Piontek[1], Georg Eckel[6], Rebecca Dischl[1,2], Raphael Märkl[1,2,†], Daniel Sauer[1], Ulrich Schumann[1], Kai Widmaier[1,2], Roger Teoh[7], Marc Stettler[7], Bastian Rauch[8], Nicolas Bellouin[3,9]

[1] Deutsches Zentrum für Luft- und Raumfahrt (DLR), Institut für Physik der Atmosphäre, Oberpfaffenhofen, Germany

[2] Johannes Gutenberg University Mainz, Institute for Atmospheric Physics, Mainz, Germany

[3] Sorbonne Université / CNRS, Institute Pierre-Simon Laplace, Paris, France

[4] National Research Council Canada, Ottawa, Canada

[5] Env-isa, Paris, France

[6] Deutsches Zentrum für Luft- und Raumfahrt (DLR), Institute of Combustion Technology, Stuttgart, Germany

[7] Department of Civil and Environmental Engineering, Imperial College London, London, UK

[8] European Union Aviation Safety Agency (EASA), Cologne, Germany

[9] University of Reading, Department of Meteorology, Reading, UK

[†] Present address: NASA Postdoctoral Program (ORAU) at NASA Langley Research Center, Hampton, VA, USA

*corresponding author: Ziming.Wang@dlr.de

Abstract. Contrail cirrus clouds are a major non-CO_2 contributor to aviation climate forcing. Current models link contrail ice particle numbers to climate impact, yet the upstream link to fuel composition remains poorly explored. Here we show that fuel hydrogen content governs soot number emissions and thereby provides a mechanistically grounded predictor of contrail ice particle numbers, with the first in-flight validation of this relationship showing agreement within ~±20%. Increasing fuel hydrogen content by 1.4 percentage points, from 13.8% to 15.2%, substantially reduces soot and ice particle numbers, contrail optical depth, lifetime and coverage, resulting in a calculated 52 [35, 67] % reduction in contrail energy forcing. Global deployment scenarios reflecting alternative fuel policies indicate substantial long-term mitigation potential from high-hydrogen content fuels. By 2050, their deployment could reduce the aviation-induced increase in global surface temperature by 21 [16, 27] %, offsetting a substantial proportion of the climate effects of projected aviation growth. Our results can establish fuel hydrogen content as a physically based metric linking fuel composition to aviation climate impacts, informing future fuel standards and mitigation strategies for climate-compatible aviation.

Introduction

Aviation plays a vital role in global connectivity and economic development, yet it contributes significantly to anthropogenic climate warming[1,2]. In addition to long-lived CO_2 emissions that persist in the atmosphere for decades[3], aviation produces substantial non-CO_2 effects, most notably contrail cirrus formed from non-volatile (soot) and volatile particles emitted during fuel combustion

in aircraft engines[4,5]. Although relatively short-lived, contrail cirrus exert an annual mean effective radiative forcing (ERF, including rapid atmospheric adjustments) comparable to that from cumulative aviation CO_2 emissions since the beginning of air traffic[6]. With global air traffic projected to more than double by 2050[7], aviation's climate footprint is expected to grow substantially. In response, many international initiatives have been introduced that may contribute to aligning aviation with the Paris Agreement temperature target[8], including market-based mechanisms to offset CO_2 growth[9], member airlines' commitments to net-zero carbon emissions by 2050[10], and governance frameworks targeting aviation non-CO_2 effects particularly contrail cirrus such as the International Civil Aviation Organization (ICAO) work programs[11] and the European Union monitoring, reporting and verification (MRV) system[12].

Contrail induced high-altitude cirrus reflect incoming solar radiation[13] and absorb outgoing infrared radiation[14]. Modulated by the presence of existing clouds[15,16,17], these processes together generally result in a net warming climate impact[18,19,20]. Contrails form when water vapour and particles, particularly soot[21,22] emitted from aviation fuel combustion freeze in the cold upper troposphere, producing ice crystals that can persist and spread into extended contrail cirrus under ice-supersaturated ambient conditions[13,23]. Accordingly, contrail mitigation has been proposed at different stages of the contrail life cycle[21], including formation through fuel composition and particle emissions, persistence and spreading[15], and detection[16] and avoidance[24].

Particle emissions during combustion depend strongly on the chemical composition of aviation fuels, which consist of mixtures of hydrocarbons with varying chain lengths and molecular structures. Paraffins with chain lengths of 8 to 15 carbon atoms constitute the majority (>75%) of conventional kerosene; their single C-C bonded hydrocarbons favor efficient combustion. Aromatic hydrocarbons, present at up to 25% of kerosene[25], contain cyclic structures that increase sooting propensity. A small fraction (~3%) of polycyclic aromatics (e.g. naphthalene) further promotes soot formation due to high molecular stability. In principle, soot emissions could be predicted from detailed fuel composition and physico-chemical combustion processes[26]. However, analytical instruments capable of resolving hydrocarbon classes and chain lengths are not yet standardized, and the hydrogen to carbon (H:C) ratios vary across hydrocarbon families. This motivates the search for a simpler composition-based parameter to characterize the fuel composition to soot particle emission relationship.

We propose fuel hydrogen content (FHC), the hydrogen mass fraction of the fuel, as a causally interpretable predictor linking fuel composition with soot particle emissions and contrail formation[26]. Ground experiments show a stronger correlation of non-volatile particulate matter (nvPM) number emissions with FHC than with aromatic content[27,28,29] (Supplementary Fig. 1), with higher FHC fuels producing fewer soot particles[30]. However, this relationship remains less well characterized under cruise conditions based on in-flight measurements[31,32]. FHC was included in early fuel specifications[33] and co-existed with other compositions such as aromatic content, but was eventually removed from specifications in favor of parameters more directly linked to operability and safety. Reintroducing FHC as a climate-relevant parameter may help constrain soot emissions and inform contrail climate impact mitigation. Because higher FHC generally correlates with lower aromatic content[27], it may also reduce CO_2 emissions per unit energy, extending mitigation beyond contrail forcing.

FHC may therefore provide a practical lever for evaluating the climate mitigation potential across aviation fuels. Conventional fossil kerosene typically has a low FHC of 13.8%. Hydroprocessing technologies can raise FHC by converting monocyclic aromatics into smaller hydrocarbons and reducing polycyclic aromatics[34]. Synthetic paraffinic kerosene (SPK), a key sustainable aviation fuel (SAF) such as hydrotreated esters and fatty acids (HEFA-SPK), is free of aromatics and exhibits high FHC[35]. Blended fuels span an FHC range of approximately 13.8–15.2%[4].

Owing to their potential to reduce aviation's lifecycle carbon footprint, the transition to alternative aviation fuels is increasingly promoted by policy, including targeting large-scale SAF production by 2030 from the U.S. SAF Grand Challenge[36] and full fuel decarbonisation by 2050, and the ReFuelEU Aviation regulation, which mandates SAF blending from 2% in 2025 to 70% by 2050[37]. The Renewable Energy Directive (RED III) also promotes synthetic fuels via the power-to-liquid (PtL) approach[38]. Complementary efforts include strengthening aviation fuel standardization[39] and evaluating fuel optimization pathways through hydroprocessing[34].

Previous global assessments have evaluated the climate impacts of alternative aviation fuel pathways[40,41,42], including the effects of SAF and liquid hydrogen on contrail cirrus ERF under future adoption scenarios[43]. However, in those studies, the contrail benefits associated with different fuels are prescribed at the pathway level – rather than derived from an observationally constrained fuel property. Here we use model-based approaches to investigate the still poorly constrained effects of fuel composition, specifically hydrogen and carbon content, on in-flight soot

emissions, contrail properties, and climate effects. We evaluate this relationship and then combine the resulting contrail and CO_2 reductions with compact Earth system model simulations to assess the implications of increasing FHC for contrail forcing, CO_2-equivalent emissions and aviation-induced warming under future fuel policy scenarios.

Results

Model evaluation with in-flight data

To assess how FHC affects emissions and contrail formation at cruise from fuel composition to climate, we simulate the 2019 European fleet (every 6th day; 1,578,734 flights) using pycontrails (version 0.54.10), i.e., the contrail model CoCiP[44] in the Python version[45], with ERA5 meteorological fields. Simulations compare the effects of a world-average reference fuel (13.8% FHC[46]; Ref) with higher FHC fuels along identical flight trajectories (Methods). The FHC–soot parameterization[46] derived for rich-quench-lean (RQL) combustors from ground-based engine tests is used, and lean-burn engines (6.5% of flights in 2019) are mapped to RQL counterparts to consider potential underestimation of ice particle numbers from volatile particle activation[5]. The parameterization is evaluated against in-flight data with different fuels from the Emission and Climate Impact of Alternative Fuels (ECLIF 1-3) campaigns for RQL engines[4,22,32] and from NEOFUELS/VOLCAN (VOL avec Carburants Alternatif Nouveaux) operated in forced rich-burn combustion mode[5,48].

Measured nvPM number emission index (EI_{nv}) from Jet A-1 is aligned with the modelled reference at the corresponding FHC, and relative reductions from alternative fuels are shown after renormalization to a common 13.8% FHC (Methods). Model results generally agree with observed nvPM emissions within experimental uncertainties across the 13.8–15.2% FHC range (Fig. 1a), and do not indicate a simple linear dependence on FHC. Positive and negative deviations from the mean FHC–soot correlation can be attributed to differences in engine type[5], operating and maintenance conditions[49], thrust settings[32,46], and degrees of engine–fuel co-optimization. Thus, soot reductions from high-FHC fuels may vary across the major in-service engine types. These factors motivate the ±20% range in EI_{nv} in the high soot regime adopted in the following sensitivity studies.

Observed reductions in the apparent contrail ice emission index EI_{ice} generally fall within the range of simulated changes in mean ice particle number N_{ice} (Fig. 1b). For the blended fuel (14.51% FHC), the measured 72% reduction in EI_{ice} exceeds that expected from FHC increases alone and is

closer to the modelled low-soot (-20%) scenario. This suggests additional effects not included in the current model, including fuel sulfur content (FSC; Supplementary Table 1), meteorological conditions, and measurement uncertainty in EI_{ice}.

Observations show that low-sulfur fuels can suppress contrail ice activation[4,22], whereas higher FSC may enhance it[47], leading to modulations in the soot-ice correlation. Models for current RQL engines generally predict a near-linear dependence between soot and contrail ice particle numbers[21,50]. Overall, our simulations are comparable to measurements for engines dominating the current fleet, and provide contrail ice particle number reductions for various fuels, forming a basis for subsequent sensitivity analyses of FHC impacts on contrail properties and climate effects.

Dependence of contrail properties and climate effects on fuel hydrogen content

Using the validated pycontrails simulations for the 2019 European fleet described above, we find that particle numbers, contrail lifetime, optical depth, coverage, and climate effects decline disproportionately with increasing FHC, with larger reductions occurring at lower FHC levels (Fig. 2a, Supplementary Table 2). This suggests that even modest increases in FHC may substantially reduce contrail impacts. Simulated contrail properties increase (decrease) under high (low)-soot emission conditions (Fig. 2b, Supplementary Table 3). For an increase in FHC from 13.8% to 15.2%, non-volatile particle numbers decrease (61%) largely driven by reduced sooting tendency associated with higher saturated hydrocarbon and more complete combustion. The potential contrail formation region slightly expands (6%), primarily attributed to higher water vapour emissions and combustion temperatures, and a weak increase in lower calorific value (LCV) per unit fuel mass. Contrail lifetime shortens (20%) because available water vapour is distributed over fewer particles, allowing them to grow larger and sediment more rapidly[4]. Reduced ice particle numbers further decrease contrail optical depth (24%) and contrail cirrus coverage (34%).

These processes substantially reduce contrail climate effects. Contrail energy forcing (EF), integrating radiative effects of contrail segments over lifetime[51], decrease by on average 52% at 15.2% FHC relative to Ref (Fig. 2c). The weak increase in LCV discussed above may slightly lower CO_2 emissions per unit energy, but contribute little to total warming reduction compared with reduced contrail EF.

The simulation results for Ref fall within the uncertainty ranges for European, North Atlantic, and global values in previous CoCiP-based studies[20,46,52]. For a 15.2% FHC representative of 100%

158 SAF, the simulated mean EF reduction of 52 [35, 67] % (Fig. 2c) is slightly larger than the 48%
159 reduction estimated in Teoh et al.[46], likely reflecting differences between pycontrails and earlier
160 CoCiP implementations and updated thrust estimates from aircraft performance models. The
161 simulated EF reduction for hydroprocessed fuels with 14.6% FHC of 39 [30, 48] % (Fig. 2c) is also
162 in close agreement with the pycontrails study of Quante et al.[34] for a narrower FHC range (14.1–
163 14.9%) using flight trajectories from Europe's five major airports. Relatively modest increases in
164 FHC to 14.6% can substantially reduce contrail forcing.

165 Contrail radiative forcing (RF) reductions inferred from the FHC–soot relationship are comparable
166 to global-scale RF estimates directly simulated by a climate model[22,53], where soot numbers are
167 prescribed and RF rather than EF is diagnosed (Fig. 2d). Differences among models arise partly
168 from cloud parameterizations[54] and meteorological conditions[55], but the overall RF reductions
169 remain broadly similar, likely reflecting microphysical scaling between ice number and contrail
170 optical depth. Simulated reductions in contrail RF are smaller than those in EF because EF
171 integrates RF over the entire contrail lifetime, whereas RF represents an instantaneous forcing rate
172 at a given contrail age. The curvature of the soot–RF dependence also differs from that of the FHC–
173 EF relationship because different physical processes contribute to each metric. RF reductions can
174 approach EF reductions for annual-mean all-sky RF (Table S11[20]). We use EF reductions here at
175 given FHC for subsequent analyses.

176 Figure 3a illustrates the processes linking fuel composition to contrail climate impact. Building on
177 the first in-flight validation of the FHC–soot number correlation, we show that slight increases in
178 FHC can lead to decreased contrail ice particle numbers and related reductions in contrail RF and
179 EF. Relative reductions in contrail RF are comparable for European[55] and global fleets[22,53] (Fig.
180 2d), providing a basis for propagating fuel composition to aviation radiative forcing, CO_2-
181 equivalence and climate response (Fig. 3b).

182 **Future aviation climate impacts shaped by fuel hydrogen content**

183 To assess global pathways towards climate-neutral aviation, we project how fuel strategies modify
184 aviation climate impacts through increases in FHC (Fig. 3c). We combine pycontrails derived
185 sensitivities of contrail forcing to FHC with OSCAR-Aviation compact Earth system model
186 simulations[56]. Contrail forcing estimates from Lee et al.[6] are constrained by scenario-specific fuel
187 use and adjusted using FHC-dependent contrail reductions derived for SAF and hydroprocessed

fuel deployment (Fig. 2c; Methods). SAF can additionally reduce CO_2 emissions[41] by up to 70%[57] (Methods). As SAF ramp up requires time, hydroprocessed fuels may offer near-term contrail mitigation potential (Fig. 2c; Methods). Figure 4 shows projected aviation CO_2 and contrail climate impacts under scenarios with evolving fuel composition according to ReFuelEU[37] and RED III[38] blending mandates, and an ICAO recommendation[58] used here to investigate a hypothetical increase in hydroprocessed fuels to a 30% share of aviation fuel use by 2050. Fuel use increases by approximately 3% annually, aside from the pandemic-related dip and recovery (Fig. 4a). SAF shares gradually increase, whereas hydroprocessed fuels expand earlier and level off, resulting in a fleet-average FHC increase of 1.2% by mid-century (Fig. 4b).

Using OSCAR-Aviation, we derive mean baselines of future efficacy-weighted ERF (ewERF) for combined contrail and CO_2-only effects under the high-emissions pathway SSP3–7.0 (Methods). Contrail ewERF is simulated based on OSCAR-Aviation by converting contrail RF using RF-based efficacy factors of 0.20[59], 0.31[60], and 0.60[61], with the average of 0.37[12,24]. CO_2 ewERF is also calculated internally by the model, and uncertainty is represented through Monte Carlo sampling. Results are shown from 2010 to 2055. Combined contrail and CO_2 forcing may decrease substantially under increasing high-FHC fuel blending (Fig. 4c). By 2050, the combined aviation forcing reduces by 30 [20, 39] %, driven largely via contrail mitigation (28%; SAF 21% and hydroprocessed fuels 7%), whereas reductions in CO_2 ewERF remain small (2%) because atmospheric CO_2 accumulates and decays only gradually[62]. In contrast, contrail ewERF responds immediately to changes in fuel composition and therefore declines from the start of fuel deployment. This points to the substantial near-term contrail mitigation potential of increasing FHC through hydroprocessed fuels during SAF scale-up.

To enable comparison of contrail and CO_2 climate effects on a common timescale, we use the efficacy-weighted[63] global warming potential[64] over a 50-year horizon (EGWP50), which accounts for the short-lived nature of contrail forcing relative to the long-term climate commitment of CO_2 (Methods). For total CO_{2e}[65] (CO_2 and contrail-specific CO_2-equivalence $CO_{2e,con}$), contrail mitigation from increasing FHC may remain the dominant contributor to climate impact reduction (Fig. 4d). By 2050, $CO_{2e,con}$ decrease by 35 [16, 55] %, of which SAF and hydroprocessed fuels contribute 30% and 6%, while direct CO_2 savings from SAF provide other 13% reduction. Given the large uncertainty, CO_{2e} may, in a pessimistic case, approach present-day $CO_{2e,con}$ levels despite continued traffic growth, or optimistically, achieve reductions broadly consistent with CORSIA

CO_2 objectives[9]. CO_2 reductions from SAF are shown separately, reflecting life cycle effects in which carbon uptake during feedstock growth and lower production emissions reduce net CO_2 emissions relative to kerosene. Lifecycle CO_2 emissions from hydroprocessed fuel production (~1–3%)[34] may slightly offset their climate benefits[66], although the overall mitigation potential remains substantial (Fig. 2c). We focus on CO_2 and contrails, and set aside other effects such as NO_x, which also depend on engine design and operating conditions. Generally, projections imply that increasing FHC could effectively reduce aviation climate impacts, particularly through contrail reduction.

To relate aviation climate impacts to temperature-based targets, we simulate near-surface warming responses using OSCAR-Aviation, driven by fuel strategy adjusted contrail ewERF and aviation CO_2 emissions (Methods). The combined deployment of hydroprocessed fuels and ReFuelEU SAF yields substantial climate mitigation potential. The similar responses of hydroprocessed fuels and the LTAG F1-Medium scenario[67] suggest that hydroprocessing provides much of the near-term increase in fleet-average FHC. By 2050, aviation-induced near-surface warming from CO_2 and contrails from the combined deployment is projected to decrease by 21% relative to the SSP3-7.0 reference scenario, with a 1σ uncertainty range [16, 27] % and a 100% probability of a positive warming reduction across Monte Carlo simulations accounting for uncertainties in climate sensitivity, carbon-cycle responses, contrail efficacy, and fuel strategy effectiveness (Fig. 2c, Fig. 5). Temperature reductions are dominated by contrail mitigation (36% of the reference contrail-induced warming). Direct CO_2 reductions contribute only 5% of baseline CO_2 warming because of the long atmospheric lifetime of CO_2, slightly lower than the relative reductions in Aamaas et al.[42] and Grewe et al.[7] due to differences in the assumed CO_2 emission reductions. Under global deployment of high-FHC fuels, contrail mitigation alone is simulated to reduce the contribution of contrails to the Paris Agreement 2°C warming goal to near present-day levels by 2050, although the combined aviation contribution remains higher, primarily due to the CO_2-induced warming (Fig. 5; Methods). Despite the promising climate mitigation potential of high-FHC fuels, multi-faceted approaches, including operational changes and advances in aircraft and engine design, remain necessary. In engine development, NO_x effects also require consideration, as their net climate impact depends on the balance between ozone production and methane depletion effects[7].

Discussion

Previous assessments have evaluated mitigation through specific fuel pathways. Here we identify FHC as a predictor linking fuel composition to particle formation and climate impacts. This single

property can be attributed to specific fuel types (e.g. SAF, PtL, or hydroprocessed fuels), independent of their origin or blending ratio. Constrained by in-flight observations across fuels and engine types, we show that increasing FHC across the observed range may result in substantial reductions in soot and contrail ice particle numbers and could halve contrail forcing. Under global fuel deployment scenarios based on current policies and recommendations, high-FHC SAF and hydroprocessed fuels with an average 1.2% increase in FHC could significantly lower aviation ewERF and CO_{2e}, and avoid about 21 [16, 27] % of contrails and aviation CO_2 induced near-surface warming by 2050.

The projected climate benefits should be interpreted in light of several limitations. Our estimates, including forcing, EGWP, and near-surface temperature responses assume global and uniform fuel implementation. Regional adoption should scale with traffic density and fuel policies and could therefore differ from the global mean calculations. Moreover, the study of near-surface temperature responses may not capture potential influences on atmospheric weather systems[68] or regional and altitude-dependent cloud adjustments.

Uncertainties also exist in the representation of particle formation processes in contrail models. The FHC–soot correlation derived for RQL combustors exhibits inherent variability across engine types, operating and maintenance conditions, introducing uncertainty into estimates of contrail ice particle numbers. As soot emissions decrease through increasing FHC and advanced combustor technologies, the relative importance of volatile particle activation is likely to increase[5,48]. This process depends on FSC and sulfate aerosol nucleation, which are not explicitly represented in many current contrail models and may either enhance[47] or suppress contrail ice formation[4,22]. Observations from emerging lean-burn combustors indicate larger ice particle number reductions than current RQL engines[5], suggesting that our estimates of future reductions are conservative. These processes require improved observational constraints and representations in future models.

Ground-based measurements have demonstrated a correlation between FHC and soot number emissions across a broad range of fuel compositions[27,28,29] (Supplementary Fig. 1). Current in-flight observations mainly constrain this relationship[46] within an FHC range of 13.8%–15.2%. Extending this relationship to hydroprocessed and other high-FHC fuels with distinct hydrocarbon compositions will require further validation with ground and flight measurements. Because contrail formation is also modulated by FSC and atmospheric temperature and relative humidity[50,69,70], broader datasets would help improve predictive capability.

These results also have practical implications for fuel producers and engine developers. Increasing FHC through fuel refining and production pathways may offer an immediate and practical opportunity to limit soot emissions and contrail climate effects. Optimization of other fuel properties, particularly sulfur content, may provide additional opportunities for contrail reduction[5]. Future engine optimization may also reduce contrail climate effects, particularly for low-soot propulsion systems, including hydrogen combustion aircraft, where contrail formation may shift towards the activation of ambient aerosols and lubrication-oil droplets[70,71,72].

These considerations may also be relevant for fuel standards and aviation climate policy. Reintroducing FHC into fuel specifications alongside aromatic content may better reflect its role in particulate emissions. Because FHC directly influences nvPM emissions regulated under ICAO CAEP standards, it may provide a measurable and trackable link between fuel composition and environmental performance. Reductions in particulate emissions may also improve airport air quality and provide health co-benefits beyond climate mitigation. As aviation policy increasingly considers non-CO_2 effects, FHC could support future monitoring and the reassessment of fuel mitigation strategies under evolving policy assumptions. More broadly, FHC can be integrated in a common framework for evaluating different fuel pathways based on a measurable fuel property. Overall, FHC offers a practical lever for reducing aviation climate, air quality and health impacts in future.

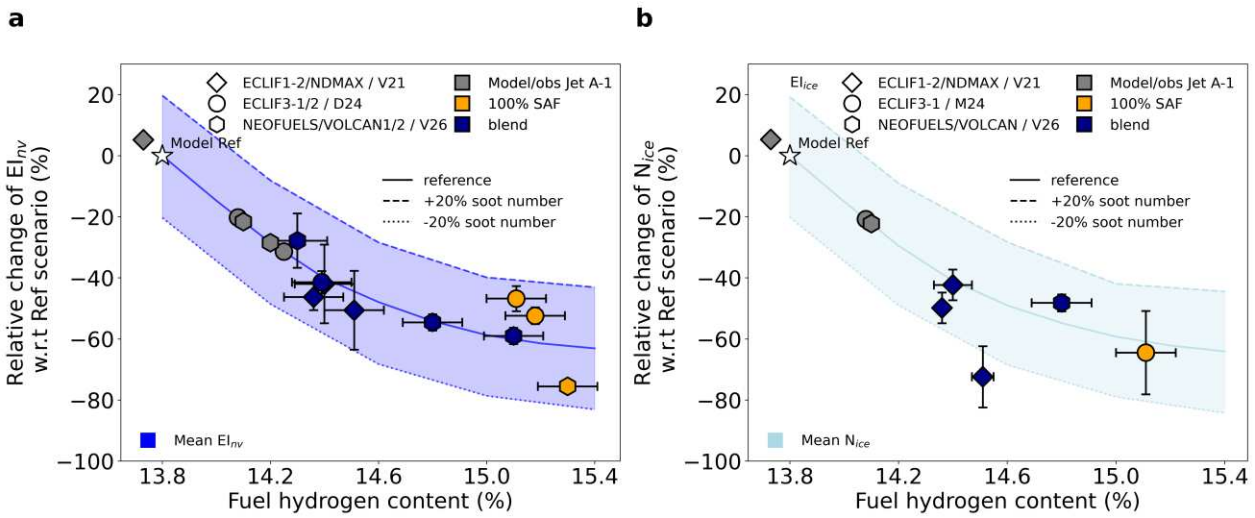


Fig. 1 | Evaluation of the correlation of aviation fuel hydrogen content with soot emission and contrail ice particle numbers using in-flight measurements. a, Relative change in emission index EI_{nv} of non-volatile soot particles as a function of fuel hydrogen content with respect to the reference value of 13.8% FHC (Ref). Solid, dashed, and dotted lines represent reference, high-, and low-soot scenarios, respectively, as simulated using pycontrails. Shaded bands indicate the range between high- and low-soot scenarios (square symbols in the legend). Aircraft measured EI_{nv} and fuel hydrogen content are shown as data points for Jet A-1 overlaid on the solid reference scenario line. EI_{nv} from alternative fuels with relative uncertainties are indicated by diamonds (ECLIF1-2; V21)[4], and circles (ECLIF3-1/2; D24)[32]. Additional measurements obtained under forced rich-burn operation of a lean-burn engine are shown as hexagons (NEOFUELS/VOLCAN1/2[5,48]; V26). The Ref fuel of 13.8% FHC[46] is indicated by a star. Fuel types are color-coded as Jet A-1 (grey), SAF (orange), and blended fuels (dark blue); detailed compositions are provided in Supplementary Table 1. **b**, Relative change in N_{ice} simulations, using the same comparison approach as in panel a and in aircraft measured EI_{ice}: diamonds (V21), circles (ECLIF3-1; M24)[22], and hexagons (V26).

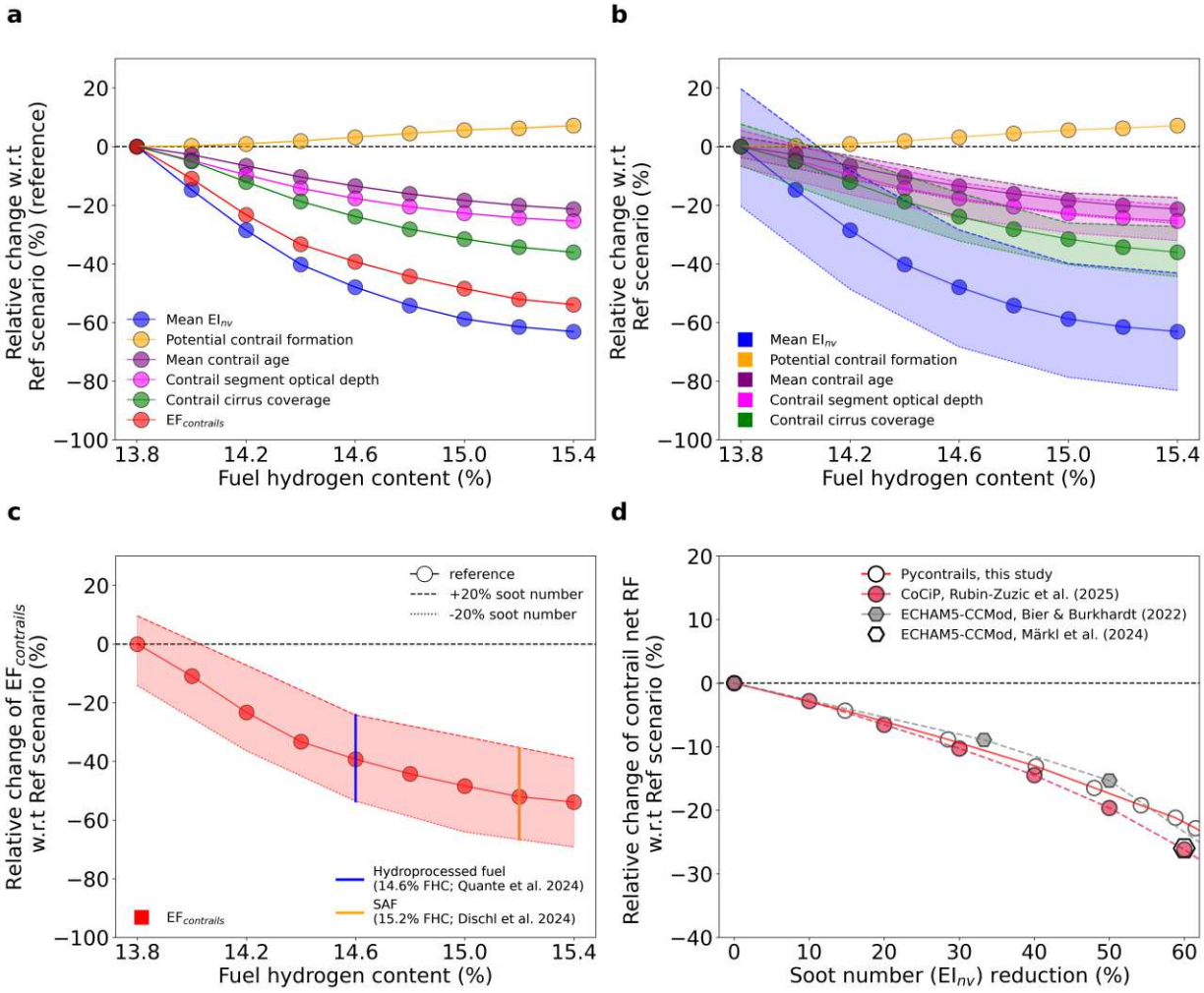


Fig. 2 | Impact of aviation fuel hydrogen content on particle emissions, contrail properties and climate effects. a, Simulations for FHC increase scenarios. Circle markers represent fleet-mean EI_{nv} (blue), potential contrail formation (orange), mean contrail age (purple), contrail segment optical depth (magenta), contrail cirrus coverage (green), and $EF_{contrails}$ (red). The black horizontal line indicates 0% change; solid lines show linear interpolation between simulated FHC levels. **b**, Simulations of particle emissions and contrail properties for high- and low-soot scenarios against the reference simulations at the same FHC, shown as shaded bands and indicated by square symbols in the legend. **c**, Simulations for $EF_{contrails}$ (as in panel b). FHC values for hydroprocessed fuels and SAF are taken from the literature, and the vertical lines indicate the $EF_{contrails}$ relative reduction range used to scale the baseline contrail forcing in Fig. 4c. **d**, Comparison of the impact of soot number (EI_{nv}) reductions on contrail cirrus net RF between model simulations, using soot reduction as the common comparison metric across studies. Results (white circle, red line) are compared with RF estimates from CoCiP (Europe)[55], and ECHAM5-CCMod (global scale)[22,53].

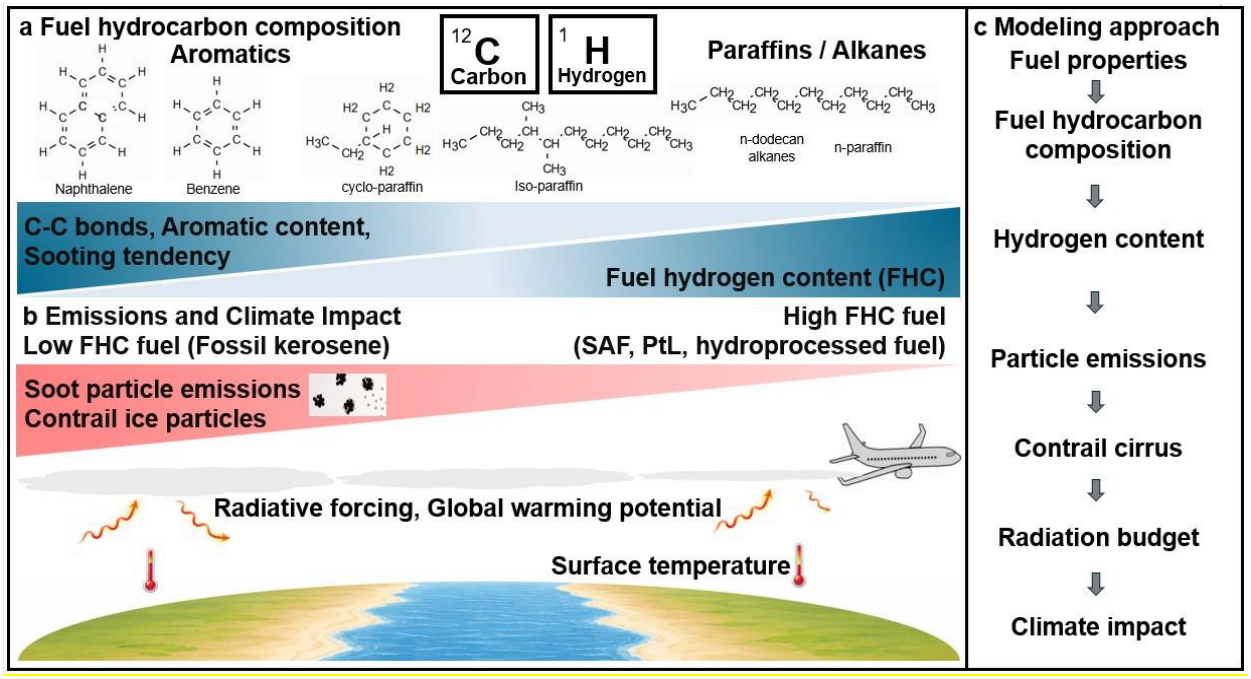


Fig. 3 | Conceptual framework linking aviation fuel composition, fuel hydrogen content, and contrail climate impacts. a, Schematic of aviation fuel hydrocarbon composition. The range involves polycyclic aromatic hydrocarbons (e.g. Naphthalene), cyclo-paraffins, and linear or branched paraffins/alkanes. Increasing hydrogen content corresponds to fewer stable C-C double bonds and lower aromatic content, and directly to a reduced sooting tendency. **b**, Emissions, contrails and their climate effects. High-FHC fuels reduce soot emissions and contrail ice particle numbers, thereby lowering contrail radiative forcing, global warming potential, and climate warming. Low-FHC fuels (fossil kerosene) exhibit the opposite behavior. **c**, Modeling approaches relating fuel properties to contrail formation, radiation budget, and future climate impacts.

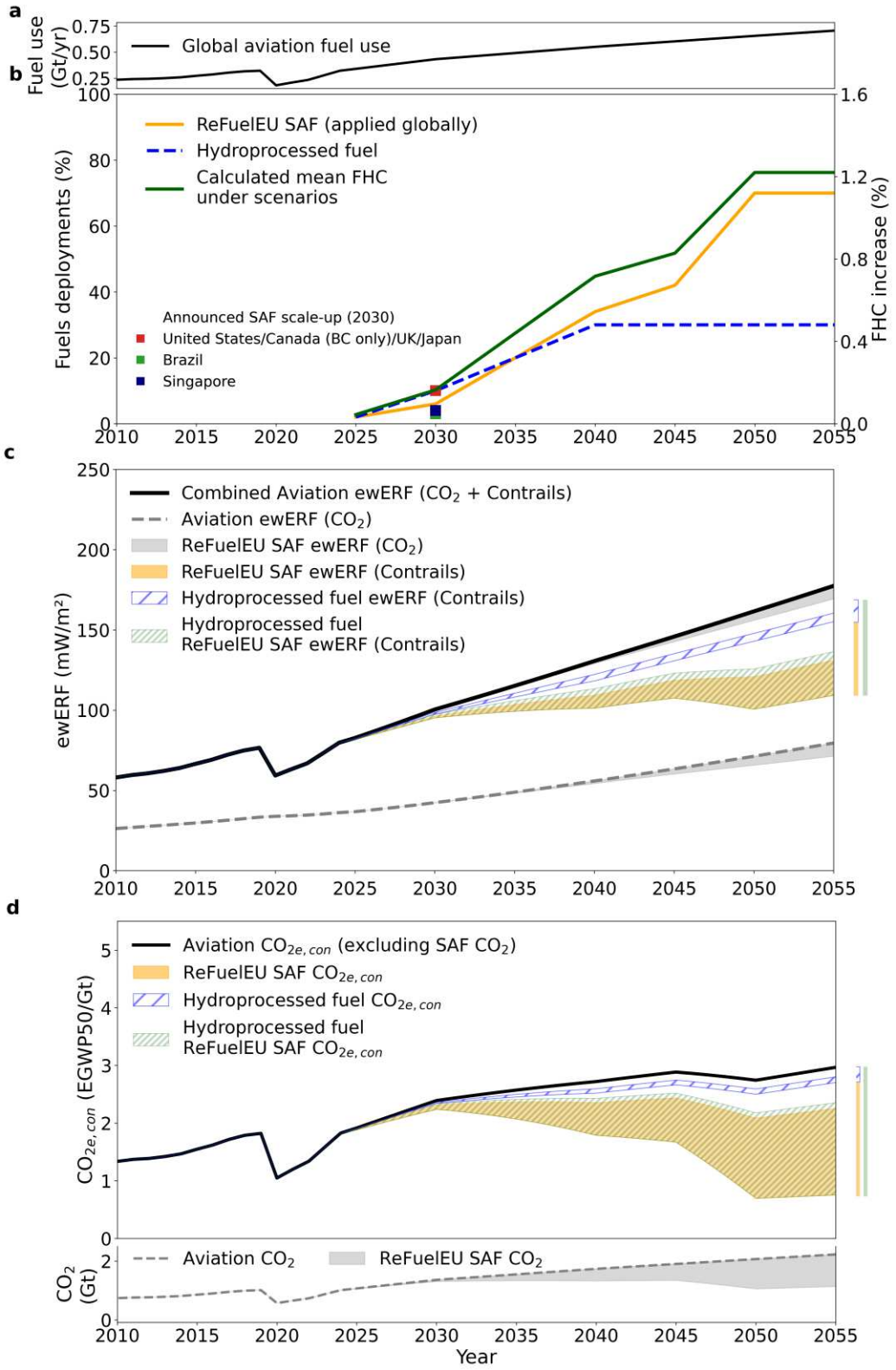


Fig. 4 | Projected aviation CO_2 and contrail effects under globally applied fuel scenarios. a, Fuel use. **b**, Fuel blending and the resulting mean FHC (ATAG announced 2030 policy). **c**,

Combined forcing from CO_2 and contrails. Solid and dashed lines represent SSP3-7.0 baselines for combined and CO_2-only effects from OSCAR-Aviation. From the combined baseline, reduction ranges are shown sequentially as shaded areas: first, CO_2 mitigation from globally applied ReFuelEU SAF (grey), followed by contrail reductions from hydroprocessed fuels (dashed blue), SAF (orange), and their combined contrail effects (dashed green). Vertical bars on the right indicate the corresponding contrail reductions. For each contribution, the uncertainty range is applied relative to the lower bound of the preceding contribution. **d**, Annual contrail-specific CO_2-equivalence ($CO_{2e,con}$) (EGWP50) and CO_2 emissions, allowing direct comparison of contrail and CO_2 climate impacts on a common metric. Lines and shaded areas show the same mitigation contributions as in panel c.

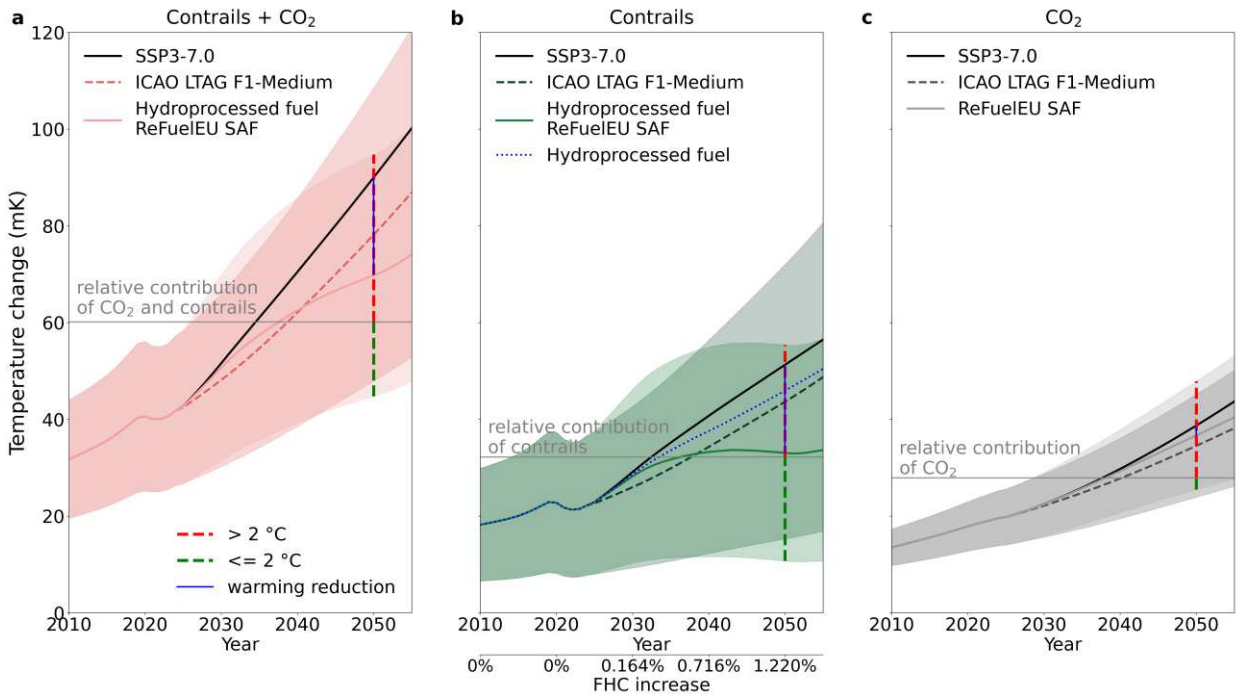


Fig. 5 | Aviation-induced near-surface temperature changes from contrails and CO_2 emissions under globally applied fuel scenarios. a-c, Temperature contributions from the combined effects of contrails and CO_2 (red), and from the separated components (color schemes consistent with Fig. 4 for the same effects) simulated with OSCAR-Aviation. Black lines indicate the reference SSP3-7.0 emission scenario. Dashed lines represent ICAO LTAG F1-Medium fuel and air-traffic growth scenario. Solid lines correspond to hydroprocessed fuel and ReFuelEU SAF scenario. The blue dotted line shows hydroprocessed fuels only. Shaded areas denote the ±1σ uncertainty ranges derived from Monte Carlo simulations. Horizontal grey lines indicate the present-day relative contributions of the combined aviation effect and individual components to the Paris Agreement 2 °C warming target. Red and green dashed vertical lines at 2050 show whether the projected relative contribution of each component is above or below its present-day value. Blue vertical lines indicate the warming reduction relative to SSP3-7.0.

Methods

Contrail modelling with CoCiP / Pycontrails

Contrails were simulated using the open-source pycontrails (version 0.54.10)[45,73], a python version of the Contrail Cirrus Prediction Model (CoCiP)[44]. Pycontrails predicts contrail formation, microphysical evolution and radiative effects for individual flights based on aircraft performance, engine emissions and meteorological conditions.

Contrail formation is diagnosed using the Schmidt–Appleman criterion (SAC). Initial ice water content, width and depth depend on aircraft characteristics and nvPM emissions. Engine nvPM emission indices were estimated using the T4/T2 scaling approach[46], which scales values from ICAO Engine Emissions Databank (v29b) according to combustor exit (T4) and inlet (T2) temperatures based on the given thrust load and is constrained by NASA ACCESS and ECLIF2 campaign data.

The FHC–soot parameterization[46] adopted in this study was derived from ground measurements for fuels with 13.8–14.9% FHC, and is extended to higher FHC values by extrapolation. Here we evaluate the correlation using in-flight measurements from ECLIF1 and, in particular, ECLIF3 and NEOFUELS/VOLCAN sampling high-FHC conditions.

Plume advection is simulated using a Lagrangian framework that accounts for ambient humidity, wind shear, and parameterized turbulence effects. Contrails persist in ice-supersaturated regions and decay through sedimentation and aggregation, with the lifetime determined by thresholds in ice particle number concentration and optical depth[20]. RF at the top of the atmosphere is calculated using an analytical parameterization derived from the libRadtran radiative transfer model[74]. Contrail overlap treatment follows the method described in Teoh et al.[20].

Model outputs include N_{ice}, potential contrail formation, contrail lifetime, optical depth, maximum contrail coverage from vertical layers, and RF. EF is calculated as $\int_0^T RF(t)L(t)W(t)dt$, where T, $L(t)$, and $W(t)$ represent the lifetime, length, and width of individual contrail segments. Outputs were aggregated from individual flights to regional and global fleet scales. Modelled EI_{ice} (per kg of fuel) can be obtained from N_{ice} (per contrail length) by normalization with fuel burn per distance (fuel flow divided by true airspeed). Because fuel burn per distance is constant under identical flight and engine conditions, relative changes in N_{ice} directly reflect relative changes in EI_{ice}. CoCiP outputs have been extensively evaluated against satellite observation-based contrail optical depth

and coverage[75], and in-situ measurements of nvPM and ice particle number[76] and contrail RF reductions during the pandemic. Regional contrail properties and climate forcing were subsequently evaluated using pycontrails simulations[20].

Aircraft performance data, including fuel consumption and propulsion efficiency, were sourced from the EUROCONTROL Base of Aircraft Data (BADA3) dataset. Engine thrusts along the flight trajectory were derived using the aircraft performance model. Flight trajectories were obtained from the 2019 Spire ADS-B dataset, including aircraft type, timing, and waypoint sequences. Simulations cover European airspace and adjacent North Atlantic regions (20°W-20°E, 35°N-60°N), including departures, arrivals and overflights. The year 2019 was chosen to represent pre-pandemic traffic levels, with simulations performed for every 6th day from 3 January to 28 December (60 days in total). The study region features one of the global highest flight densities together with a wide range of meteorological conditions.

Meteorological fields were obtained from the ERA5 reanalysis produced by the European Centre for Medium-Range Weather Forecasts. Temperature and humidity determine contrail formation and persistence. Relative humidity over ice (RHi) was corrected following Teoh et al.[52] to account for known upper-tropospheric humidity biases. ERA5 IWC is used to represent background cirrus conditions and to account for cloud–contrail overlap effects in the radiative calculations. ERA5 data have 0.25° horizontal resolution, hourly temporal frequency and pressure-level vertical spacing, covering typical cruise altitudes (200-400 hPa).

Pycontrails (version 0.54.10) simulations were performed for the 2019 European fleet on every 6th day of the year, covering 1,578,734 flights (Supplementary Fig. 2) to represent annual traffic and weather patterns while maintaining computational efficiency. Contrail properties were simulated for a world-average reference fuel with 13.8% FHC (Ref) and for fuels with increasing FHC using identical flight trajectories and meteorological conditions.

Fuel hydrogen content and soot number emissions scenarios

Reference scenario: The baseline case (Ref) represents simulations for Jet A-1 fuel with 13.8% FHC, with soot emissions derived based on ICAO EDB[46]. Soot activation follows a temperature-dependent parameterization constrained by measurements between the SAC and ambient temperatures[69].

FHC increase scenarios: Relative changes in contrail properties were evaluated by incrementally increasing FHC from 14.0% to 15.4% in 0.2% steps (eight scenarios). For each scenario, pycontrails simulations produced changes in EI_{nv}, contrail ice particle number, potential contrail formation, age, optical depth, contrail cirrus coverage, RF, and EF. Increasing FHC implies a corresponding reduction in aromatic content.

High- and low-soot sensitivity scenarios: Additional sensitivity simulations explored variability in soot numbers. High- and low-soot scenarios were implemented by adjusting soot number emissions by ±20% across the same FHC range (13.8–15.4%) and FHC increments (0.4%), with the low-soot scenarios representing reduced ice activation from lower soot number emissions or reduced FSC.

Uncertainty and renormalization of particle number measurements

Measurements of EI_{nv} and EI_{ice} were compiled from multiple flight campaigns covering a range of fuels, engine types, and operating conditions[4,5,22,32]. The overall uncertainty in EI_{nv} is at 15% during ECLIF1. The uncertainty of near-field aerosol measurements during ECLIF3 and VOLCAN campaigns was approximately 10%. The uncertainties of far-field EI_{ice} measurements were approximately 33% and 20%, respectively. The FHC testing uncertainty for ECLIF1-2 is recorded in Table 1 of Voigt et al.[4] and is 0.11% for all tested fuels during the ECLIF3 and NEOFUELS/VOLCAN campaigns.

For each campaign, particle number reductions, $\Delta N(FHC_{cont})$, were relative to the campaign-specific Jet A-1 reference fuel with FHC0. Here ΔN denotes the reduction either in EI_{nv} or EI_{ice}.

To compare these observations with the parameterization of Teoh et al.[46], which defines reductions relative to a reference fuel with 13.8% FHC, measured reductions were renormalized to this common reference. Let $\Delta N_{FHC0}(FHC_{cont})$ denote the measured percent reduction relative to the campaign reference fuel of FHC0, and $\Delta N_{13.8}(FHC0)$ represents the simulated percent reduction at the campaign reference FHC0 relative to 13.8% FHC. The corresponding reduction relative to the 13.8% FHC is obtained as

$$\Delta N_{13.8}(FHC_{cont}) = 100\left[\left(1 + \frac{\Delta N_{FHC0}(FHC_{cont})}{100}\right)\left(1 + \frac{\Delta N_{13.8}(FHC0)}{100}\right) - 1\right] \quad (1)$$

This transformation expresses measurements and model parameterizations relative to a common reference fuel, ensuring consistent comparison of particle number reductions across campaigns with different baseline Jet A-1 FHC.

OSCAR-Aviation baseline aviation climate forcing

Future aviation climate responses were simulated using OSCAR-Aviation, an aviation-specific extension of the reduced-complexity Earth system model OSCAR[56]. OSCAR represents key components of the climate system, including the carbon cycle, atmospheric chemistry, aerosols, and surface albedo, and simulates ERF and global and regional temperature responses from pre-industrial periods to future scenarios using impulse-response functions that approximate the thermal inertia of the climate system.

OSCAR-Aviation extends this model to represent aviation-specific climate forcings. Baseline contrail ewERF supplied to OSCAR-Aviation was derived by first scaling the global 2018 contrail RF estimate of 111.4 (33-189) mWm^{-2} from Lee et al.[6] with annual aviation fuel use. Aviation fuel consumption was inferred from CMIP6 ScenarioMIP aviation CO_2 emissions under SSP3-7.0 using an emission index of 3.16 kg CO_2 per kg of fuel, with pandemic-related reductions and recovery in aviation activity incorporated following Dannet et al.[77]. Because neither pycontrails nor OSCAR-Aviation explicitly resolves rapid atmospheric adjustments associated with contrail forcing, RF was converted to ewERF using RF-based efficacy factors. To propagate efficacy uncertainty, contrail efficacies of 0.20[59], 0.31[60], and 0.60[61] were sampled within the Monte Carlo simulations, spanning the mean efficacy of 0.37[12,24]. Although the recent estimate of 0.20 from Bickel et al.[59] may represent a lower-bound constraint owing to nonlinear saturation effects in high-traffic simulations, all three efficacy values were retained to propagate uncertainty. The global contrail RF estimate of 62 mWm^{-2} for 2019 from pycontrails simulations[20] lies within the uncertainty range in Lee et al.[6] for 2018, although the updated pycontrails version used here does not exactly reproduce the results of Teoh et al.[20].

$$ewERF^{(i)}_{contr,SSP}(t) = M_{contr}(RF_{Lee}, fuel_{SSP}(t), \varepsilon^{(i)};\ \theta^{(i)}) \quad (2)$$

where M_{contr} denotes the OSCAR-Aviation contrail-forcing module, $\varepsilon^{(i)}$ the sampled contrail efficacy, and $\theta^{(i)}$ the (i)-th realization of Earth-system parameters.

Aviation CO_2 forcing was calculated using OSCAR's multi-box carbon-cycle representation coupled with the RF formulation. Baseline aviation CO_2 emissions were obtained from ScenarioMIP under SSP3-7.0 and propagated through OSCAR-Aviation to compute the resulting CO_2 ewERF. For each Monte Carlo realization (i),

$$ewERF^{(i)}_{co_2,SSP}(t) = M_{CO_2}(E_{CO_2,SSP}(t);\ \theta^{(i)}) \quad (3)$$

where M_{CO_2} denotes the OSCAR-Aviation carbon-cycle and CO_2-forcing module. For CO_2, efficacy was assumed to be unity, such that ewERF was obtained directly from OSCAR-Aviation.

$$\overline{ewERF}(t) = \langle ewERF^{(i)}(t)\rangle_i \quad (4)$$

Ensemble mean and uncertainty in both baseline contrail and CO_2 ewERF was quantified using 200 Monte Carlo simulations with perturbed Earth system parameters, including equilibrium climate sensitivity, ocean heat uptake, carbon-cycle response and etc.

Fuel strategies

Fuel-based mitigation scenarios were implemented by modifying the baseline contrail forcing and aviation CO_2 emissions described above according to projected SAF and hydroprocessed fuel deployment. Contrail mitigation was represented using relative forcing reductions derived from the 2019 pycontrails simulations for increasing FHC (Fig. 2c), while aviation CO_2 emissions were adjusted using lifecycle emission reductions associated with SAF.

SAF deployment

SAF adoption is assumed to follow the ReFuelEU Aviation mandates globally, with blending ratios of 2% (2025), 6% (2030), 20% (2035), 34% (2040), 42% (2045) and 70% (2050), remaining constant thereafter.

Contrail reductions were implemented by scaling the baseline contrail ewERF from OSCAR-Aviation using relative forcing reductions (δ) derived from the 2019 pycontrails simulations with $p_{SAF}(t) \cdot \delta_{SAF,contrail}$ as $R_{SAF,contrail}(t)$:

$$ewERF_{contrail,SAF}(t) = \overline{ewERF_{contrail}(t)} \cdot \left(1 - R_{SAF,contrail}(t)\right) \quad (5)$$

where $p_{SAF}(t)$ is the SAF blending fraction in year (t), and $\delta_{SAF,contrail} \in [0.35, 0.67]$ represents the simulated contrail forcing reduction for fuels with 15.2% FHC, representative of 100% SAF, relative to the "Ref" fuel between high- and low-soot conditions (Fig. 2c).

Aviation CO_2 emissions under SAF deployment were calculated as

$$E_{CO_2,SAF}(t) = E_{CO_2}(t) \cdot \left(1 - p_{SAF}(t) \cdot \delta_{SAF,CO_2}\right) \quad (6)$$

where $E_{CO_2}(t)$ denotes the baseline SSP3-7.0 aviation CO_2 emissions, and $\delta_{SAF,CO_2} \in [0, 0.7]$ represents the reduction range of lifecycle CO_2 emission related to SAF use[57]. This range reflects uncertainties related to feedstock type, production pathway, and energy supply, referring to estimated based on Eqs. (1)-(2) and Table 1-2 in Aamaas et al.[42]. For the uncertainty analysis, the reduction factor was randomly sampled within this range, meaning that the 70% reduction represents an upper-bound estimate rather than a typical value.

Hydroprocessed fuel deployment

A hypothetic hydroprocessed fuel adoption scenario was implemented independently, assuming that an increasing fraction of kerosene is hydroprocessed to increase FHC to 14.6%, corresponding to the midpoint between mild and harsh hydroprocessing levels[34]. The hydroprocessed share $p_{hydro}(t)$ of aviation fuels reaches 2% (2025), 10% (2030), 20% (2035) and 30% (2040), remaining constant thereafter. Combined with the ReFuelEU-based SAF deployment, the fleet-average FHC reaches approximately 15.0% by 2050.

Hydroprocessed fuels are assumed not to reduce CO_2 emissions but to reduce contrail forcing. The relative contrail forcing reduction factor, $\delta_{hydro,contrail} \in [0.30, 0.48]$, is derived from simulations for 14.6% FHC (Fig. 2c), relative to the "Ref" fuel under high- and low-soot conditions. $R_{hydro,contrail}(t)$ and $ewERF_{contrail,hydro}(t)$ was calculated analogously to Eq. (5).

To propagate uncertainties in mitigation effectiveness to temperature responses, equivalent fuel usages were generated for Monte Carlo realizations based on Aamaas et al.[42],

$$fuel_{total,SAF\&hydro}(t) = \left(\frac{fuel_{jet}(t)}{fuel_{total}(t)} \cdot \left(1 - R_{\mathrm{SAF,contrail}}(t) - R_{\mathrm{hydro,contrail}}(t)\right) + \right.$$

$$\left. \frac{fuel_{SAF}(t)}{fuel_{total}(t)} \cdot R_{\mathrm{SAF,contrail}}(t) + \frac{fuel_{hydro}(t)}{fuel_{total}(t)} \cdot R_{\mathrm{hydro,contrail}}(t)\right) \quad (7)$$

$fuel_{total,hydro}(t)$ was calculated analogously. These fuel usages and corresponding aviation CO_2 emissions were then used as inputs to OSCAR-Aviation to estimate fuel adjusted near-surface temperature responses.

Temperature response simulations with OSCAR-Aviation

For the temperature simulations shown in Fig. 5, OSCAR-Aviation was driven by aviation CO_2 emissions and contrail forcing under SSP3-7.0 as the baseline scenario, together with the ICAO Long-Term Aspirational Goal (LTAG) F1-Medium scenario (50% SAF blend ratio; 3.6%/year traffic growth)[67], the combined hydroprocessed fuel and ReFuelEU SAF strategy, and the hydroprocessed fuel strategy alone. Climate response uncertainties were quantified using the same 200-member Monte Carlo ensemble described above, such that uncertainties in Earth system parameters, and contrail efficacy and fuel strategy effectiveness were propagated consistently from baseline forcing estimates to temperature response simulations.

$$T_s^{(i)}(t) = M_T(fuel_s^{(i)}(t), E_{CO_2,s}^{(i)}(t), \varepsilon^{(i)};\ \theta^{(i)}) \qquad (8)$$

where *s* denotes SSP3-7.0, LTAG F1-Medium, the combined ReFuelEU SAF and hydroprocessed fuel scenario, and the hydroprocessed fuel scenario, respectively, where M_T denotes the OSCAR-Aviation temperature-response module, $fuel_s^{(i)}(t)$ the fuel use for scenario (s), $E_{CO_2,s}^{(i)}(t)$ the corresponding aviation CO_2 emissions, $\varepsilon^{(i)}$ the sampled contrail efficacy, and $\theta^{(i)}$ the (t)-th realization of Earth-system parameters.

$$R_s^{(i)}(t) = \frac{T_{SSP}^{(i)}(t) - T_s^{(i)}(t)}{T_{SSP}^{(i)}(t)} \times 100$$

$$\overline{R_s}(t) = \langle R_S^{(i)}(t) \rangle_i,\ \sigma_{R_s}(t) = std_i\left[R_S^{(i)}(t)\right] \qquad (9)$$

where $R_s^{(i)}(t)$ is the percentage reduction in aviation-induced warming for scenario *s* relative to the SSP3-7.0 reference scenario for Monte Carlo realization *i*, and $\sigma_{R_s}(t)$ represents the corresponding ensemble standard deviation.

To contextualize aviation-induced warming relative to the Paris Agreement temperature targets, the simulated warming contributions of aviation CO_2 and contrail under SSP3-7.0 were expressed relative to the observed global warming of +1.42 °C in 2025 above pre-industrial levels[17,78]. Under this framing, contrails and aviation CO_2 correspond to approximately 1.61 % and 1.40 % of the 2 °C warming threshold, respectively, yielding a combined aviation-induced warming equivalent to 3.01 % of the 2 °C target. These relative contributions are projected to increase toward mid-century[7]. Future fuel strategies were evaluated against present-day aviation-induced warming to

assess if they could offset continued growth in aviation activity and reduce aviation-induced warming below its current relative contribution.

Climate metrics

To express aviation CO_2 and contrail impacts and mitigation within a common climate metric, we computed the efficacy-weighted global warming potential over a 50-year horizon (EGWP50) following Teoh et al.[20].

For CO_2 emissions, the 50-year absolute global warming potential $AGWP50_{CO_2} = 5.35 \times 10^{-14} Wm^{-2} yr\, kg_{CO_2}^{-1}$ [62] was used to compute EF from emitted CO_2 mass M_{CO_2}:

$$EF_{CO_2} = AGWP50_{CO_2} \cdot M_{CO_2} \cdot A \cdot t \qquad (10)$$

where A (m^2) is Earth's surface area and t the number of seconds per year.

The EGWP50 metric for contrail (mitigation) was calculated as

$$EGWP50 = \frac{ewERF_{contr} \cdot A \cdot t}{EF_{CO_2}} \qquad (11)$$

where $ewERF_{contr}$ is the annual-mean ERF of contrails obtained from OSCAR-Aviation simulations.

CO_2-equivalent emissions ($CO_{2e,con}$, kg) from contrail contributions were then derived using EGWP50:

$$CO_{2e,con} = M_{CO_2} \cdot EGWP50 \qquad (12)$$

This framework was applied to baseline and mitigation scenarios (hydroprocessed fuel and ReFuelEU SAF) to generate annual time series of aviation CO_{2e} with a 50-year integration horizon.

Acknowledgements The authors acknowledge the computational and data resources provided through the joint high-performance data analytics (HPDA) project "terrabyte" of the German Aerospace Center (DLR) and the Leibniz Supercomputing Center (LRZ). The authors thank Simon Christie for providing the ground measurements of black carbon number and FHC from the EU Horizon project JETSCREEN (grant no. 723525) used in Supplementary Fig. 1. The authors also thank Luca Bugliaro for discussions on the simulation scenarios and model results, and Volker Grewe for discussions on the presentation of the manuscript and the interpretation of climate metrics. ZW acknowledges funding from the EU Horizon projects PACIFIC (grant no. 101192234) and A4CLIMATE (grant no. 101192301). CV acknowledges funding from the DFG projects ECOCON (grant no. 510826369), HALO (grant no. 316646266) and MJ and SK acknowledge funding from A4CLIMATE. AM and GS acknowledge funding from the European Aviation Fuel Standards Project (grant no. EASA.2023.FC02). AL, NB, and ZW were supported by the French Ministère de la Transition Écologique et Solidaire through the Climaviation project (grant no. DGAC N2021-39), with additional support from France's Plan National de Relance et de Résilience (PNRR) and the European Union's NextGenerationEU.

Author Contributions ZW and CV conceptualized the study. ZW and AM designed the FHC simulation scenarios supervised by CV with feedback from GS and BR. ZW and AM conducted the pycontrails simulations, ZW performed the data analysis, and AM extracted Supplementary Fig. 2. AL provided the "OSCAR-Aviation" code and emission inventory. ZW completed "OSCAR-Aviation" simulations and ZW, NB and AL interpreted the metrics. JM initiated the projections shown in Fig. 4c and d. SK, DP, KW, and JM developed and maintained the DLR pycontrails framework. RD, RM, CV, and DS performed the in-flight measurements and analysed the aerosol and cloud data. US developed the CoCiP model, and RT and MS developed the parameterization linking nvPM number emissions to FHC. GS and GE contributed expertise on engine emissions and fuel chemistry. ZW wrote the manuscript. All authors commented on and contributed to the manuscript.

Competing Interests

The authors declare that they have no competing interests.

Data Availability

The pycontrails simulation output required to reproduce Figs. 1 and 2 are provided at Supplementary Tables 1-3. The OSCAR-Aviation outputs related to Figs. 4 and 5 are available as two Excel files deposited at Zenodo [https://doi.org/10.5281/zenodo.21346201].

Code Availability

The pycontrails repository that contains the CoCiP model is available at https://py.contrails.org/index.html. The OSCAR compact Earth system model is available at https://github.com/tgasser/OSCAR.

References

1. Boucher, O., Randall, D., Artaxo, P. et al. (eds.) Climate Change 2013: The Physical Science Basis. Contribution of Working Group I to the Fifth Assessment Report of the Intergovernmental Panel on Climate Change, pp. 571–658, https://doi.org/10.1017/CBO9781107415324.016 (2013).

2. Brasseur, G.P., Gupta, M., Anderson, B.E. et al. Impact of Aviation on Climate: FAA's Aviation Climate Change Research Initiative (ACCRI) Phase II. *Bull. Amer. Meteor. Soc.* **97**(4), 561–583, https://doi.org/10.1175/BAMS-D-13-00089.1 (2016). 3. IPCC: Climate Change 2023: Synthesis Report. Contribution of Working Groups I, II and III to the Sixth Assessment Report of the Intergovernmental Panel on Climate Change [Core Writing Team, H. Lee and J. Romero (eds.)]. IPCC, Geneva, Switzerland, pp. 35-115, https://doi.org/10.59327/IPCC/AR6-9789291691647 (2023).

4. Voigt, C., Kleine, J., Sauer, D. et al. Cleaner burning aviation fuels can reduce contrail cloudiness. *Commun Earth Environ* **2**, 114, https://doi.org/10.1038/s43247-021-00174-y (2021).

5. Voigt, C., Märkl, R., Sauer, D. *et al.* Substantial aircraft contrail formation at low soot emission levels. *Nature* **652**, 112–118, https://doi.org/10.1038/s41586-026-10286-0 (2026).

6. Lee, D. S. et al. The contribution of global aviation to anthropogenic climate forcing for 2000 to 2018. *Atmos. Environ* **244**, 117834 (2021).

7. Grewe, V., Gangoli Rao, A., Grönstedt, T. et al. Evaluating the climate impact of aviation emission scenarios towards the Paris agreement including COVID-19 effects. *Nat Commun* **12**, 3841, https://doi.org/10.1038/s41467-021-24091-y (2021).

8. UNFCCC. Paris Agreement. https://unfccc.int/process-and-meetings/the-paris-agreement/the-paris-agreement. United Nations Framework Convention on Climate Change (2015)

9. ICAO. Annex 16 to the Convention on International Civil Aviation, Environmental Protection, Vol. IV Carbon Offsetting Scheme for International Aviation (CORSIA), First Edition, October 2018, ISBN 978-92-9258-611-9 (2018).

10. IATA. Resolution on the industry's commitment to reach net zero carbon emissions by 2050, https://www.iata.org/contentassets/dcd25da635cd4c3697b5d0d8ae32e159/iata-agm-resolution-on-net-zero-carbon-emissions.pdf (2021).

11. ICAO. ICAO Symposium on Non-CO_2 Aviation Emissions, https://www.icao.int/events/2024-icao-symposium-non-co2-aviation-emissions (2024).

12. EU. Non-CO2 Monitoring Reporting and Verification System. https://climate.ec.europa.eu/document/download/2efafc7e-8b25-4763-906f-a7ba23b466d2_en?filename=policy_ets_avaiation_explainer_non-co2_mrv_tasks_for_ao_en.pdf (2025).

13. Wang, Z., Bugliaro, L., Jurkat-Witschas, T. et al. Observations of microphysical properties and radiative effects of a contrail cirrus outbreak over the North Atlantic. *Atmos. Chem. Phys.* **23**, 1941–1961, https://doi.org/10.5194/acp-23-1941-2023 (2023).

14. Burkhardt, U. & Kärcher, B. Global radiative forcing from contrail cirrus. *Nature Clim Change* **1**, 54–58 (2011).

15. Petzold, A., Khan, N.F., Li, Y. *et al.* Most long-lived contrails form within cirrus clouds with uncertain climate impact. *Nat Commun* **16**, 9695, https://doi.org/10.1038/s41467-025-65532-2 (2025).

16. Seelig, T., Wolf, K., Bellouin, N. *et al.* Quantification of the radiative forcing of contrails embedded in cirrus clouds. *Nat Commun* **16**, 10703, https://doi.org/10.1038/s41467-025-66231-8 (2025).

17. Wang, Z. & Voigt, C. Tracing contrails within cirrus clouds and their climate effect. *Nat Commun* **16**, 10702, https://doi.org/10.1038/s41467-025-66724-6 (2025).

18. Gettelman, A., Chen, C.-C., & Bardeen, C. G. The climate impact of COVID-19-induced contrail changes. *Atmos. Chem. Phys.* **21**, 9405–9416, https://doi.org/10.5194/acp-21-9405-2021 (2021).

19. Quaas, J., Gryspeerdt, E., Vautard, R. et al. Climate impact of aircraft-induced cirrus assessed from satellite observations before and during COVID-19. *Environ. Res. Lett.* **16**, 064051, https://doi.org/10.1088/1748-9326/abf686 (2021)

20. Teoh, R., Engberg, Z., Schumann, U. et al. Global aviation contrail climate effects from 2019 to 2021. *Atmos. Chem. Phys.* **24**, 6071–6093, https://doi.org/10.5194/acp-24-6071-2024 (2024).

21. Kärcher, B. Formation and radiative forcing of contrail cirrus. *Nat Commun* **9**, 1824, https://doi.org/10.1038/s41467-018-04068-0 (2018).

22. Märkl, R. S., Voigt, C., Sauer, D. et al. Powering aircraft with 100 % sustainable aviation fuel reduces ice crystals in contrails. *Atmos. Chem. Phys*. **24**, 3813–3837, https://doi.org/10.5194/acp-24-3813-2024 (2024).

23. Wang, Z., Bugliaro, L., Gierens, K. et al. Machine learning for improvement of upper-tropospheric relative humidity in ERA5 weather model data. *Atmos. Chem. Phys.* **25**, 2845–2861, https://doi.org/10.5194/acp-25-2845-2025 (2025).

24. Kirschler, S., Voigt, C., Piontek, D. et al. Towards climate compatible aviation: operational feasibility of contrail avoidance by flight path adjustments. Preprint at https://doi.org/10.21203/rs.3.rs-8799231/v1.

25. ASTM D1655. Standard Specification for Aviation Turbine Fuels, https://store.astm.org/d1655-24.html (2024).

26. EASA. The Aviation Non-CO2 Experts Network (ANCEN) as part of NONCO2 Research Project Background Note, Benefits of changes in fuel composition on aviation non-CO2 emissions, https://www.easa.europa.eu/en/research-projects/ancen-nonco2 (2026).

27. Brem, B.T., Durdina, L., Siegerist, F. et al. Effects of Fuel Aromatic Content on Nonvolatile Particulate Emissions of an In-Production Aircraft Gas Turbine. *Environ Sci Technol* **2015**, 49, 13149–57, https://doi.org/10.1021/acs.est.5b04167 (2015).

28. Durand, E., Lobo, P., Crayford, A. et al. Impact of fuel hydrogen content on non-volatile particulate matter emitted from an aircraft auxiliary power unit measured with standardised reference systems. *Fuel*. **287**, 119637, https://doi.org/10.1016/j.fuel.2020.119637 (2021).

675 29. Schripp, T., Anderson, B. E., Bauder, U. et al. Aircraft engine particulate matter emissions from sustainable aviation
676 fuels: Results from ground-based measurements during the NASA/DLR campaign ECLIF2/ND-MAX. *Fuel*. **325**,
677 124764, https://doi.org/10.1016/j.fuel.2022.124764 (2022).

678 30. Beyersdorf, A. et al. Reductions in aircraft particulate emissions due to the use of Fischer–Tropsch fuels. *Atmos.*
679 *Chem. Phys.* **14**, 11–23, https://doi.org/10.5194/acp-14-11-2014 (2014).

680 31. Moore, R., Thornhill, K., Weinzierl, B. et al. Biofuel blending reduces particle emissions from aircraft engines at
681 cruise conditions. *Nature* **543**, 411–415, https://doi.org/10.1038/nature21420 (2017).

682 32. Dischl, R., Sauer, D., Voigt, C. et al. Measurements of particle emissions of an A350-941 burning 100 % sustainable
683 aviation fuels in cruise. *Atmos. Chem. Phys*. **24**, 11255–11273, https://doi.org/10.5194/acp-24-11255-2024 (2024).

684 33. DERD 2494 Issue 8. Specification for Aviation Turbine Fuel (Kerosine Type). UK Ministry of Defence, Directorate
685 of Engine Research and Development (DERD), London (1978).

686 34. Quante, G., Voß, S., Bullerdiek, N. et al. Hydroprocessing of fossil fuel-based aviation kerosene – Technology
687 options and climate impact mitigation potentials. *Atmospheric Environment: X* **22**, 100259,
688 https://doi.org/10.1016/j.aeaoa.2024.100259 (2024).

689 35. ASTM D7566. Standard Specification for Aviation Turbine Fuel Containing Synthesized Hydrocarbons,
690 https://store.astm.org/d7566-24.html (2024).

691 36. SAF Grand Challenge Roadmap. Flight Plan for Sustainable Aviation Fuel,
692 https://www.energy.gov/sites/default/files/2022-09/beto-saf-gc-roadmap-report-sept-2022.pdf (2022).

693 37. EU. ReFuel EU Initiative, https://transport.ec.europa.eu/transport-modes/air/environment/refueleu-aviation_en
694 (2023a).

695 38. EU. Renewable Energy Directive. https://energy.ec.europa.eu/topics/renewable-energy/renewable-energy-
696 directive-targets-and-rules/renewable-energy-directive_en (2023b).

697 39. EASA. The "European body for jet fuel standards and safety certification" pilot project.
698 https://www.easa.europa.eu/en/newsroom-and-events/press-releases/easa-hosts-first-eu-aviation-fuel-stakeholder-
699 forum (2024).

700 40. Brazzola, N., Patt, A. & Wohland, J. Definitions and implications of climate-neutral aviation. *Nat. Clim. Chang.* **12**,
701 761–767, https://doi.org/10.1038/s41558-022-01404-7 (2022).

702 41. Dray, L., Schäfer, A.W., Grobler, C. et al. Cost and emissions pathways towards net-zero climate impacts in
703 aviation. *Nature Clim Change* **12**, 956–962, https://doi.org/10.1038/s41558-022-01485-4 (2022).

704 42. Aamaas, B., Lund, M. T., Fuglestvedt, J. S. et al. Continued global warming from aviation even under high-
705 ambition mitigation scenarios. *One Earth* **8**, https://doi.org/10.1016/j.oneear.2025.101451 (2025).

706 43. Zhang, W., Feng, W., Dray, L. et al. Strong simulated reductions in contrail cirrus effective radiative forcing from
707 alternative fuels. Preprint at https://doi.org/10.21203/rs.3.rs-9853842/v1.

44. Schumann, U. A contrail cirrus prediction model. *Geosci. Model Dev*. **5**, 543–580, https://doi.org/10.5194/gmd-5-543-2012 (2012).

45. Engberg, Z., Teoh, R., Abbott, T. et al. Forecasting contrail climate forcing for flight planning and air traffic management applications: the CocipGrid model in pycontrails 0.51.0. *Geosci. Model Dev*. **18**, 253–286, https://doi.org/10.5194/gmd-18-253-2025 (2025).

46. Teoh, R., Schumann, U., Voigt, C. et al. Targeted Use of Sustainable Aviation Fuel to Maximize Climate Benefits. *Environ Sci Technol* **56**, 17 246–15 255, https://doi.org/10.1021/acs.est.2c05781 (2022a).

47. Dischl, R., Märkl, R., Sauer, D. *et al.* Fuel sulfur content can modulate contrail ice crystal numbers. *Commun Earth Environ* **6**, 902, https://doi.org/10.1038/s43247-025-02951-5 (2025).

48. Dischl, R., Sauer, D., Voigt, C. et al. Mitigating aviation's environmental impact through alternative fuels and cleaner engines. *Sci. Adv.* (in press), https://doi.org/10.1126/sciadv.aeg7503 (2026).

49. Apostolidis, A. & K. P. Stamoulis. A Health Monitoring Modelling Case Study: Humidity Effects on Engine Deterioration Prediction. In: MATEC Web of Conferences 349. Ed. by S. Pantelakis, G. Lampeas, and K. Tserpes, p. 03011. issn: 2261-236X (2021).

50. Yu, F., Kärcher, B. & Anderson, B. E. Revisiting contrail ice formation: Impact of primary soot particle sizes and contribution of volatile particles. *Environ Sci Technol* **58**, 17650–17660, https://doi.org/10.1021/acs.est.4c04340 (2024).

51. Schumann, U., Graf, K. & Mannstein, H. Potential to reduce the climate impact of aviation by flight level changes. In Proc. 3rd AIAA Atmospheric Space Environments Conference (2011).

52. Teoh, R., Schumann, U., Gryspeerdt, E. et al. Aviation contrail climate effects in the North Atlantic from 2016 to 2021, *Atmos. Chem. Phys*. **22**, 10 919–10 935, https://doi.org/10.5194/acp-22-109192022 (2022b).

53. Bier, A., & Burkhardt, U. Impact of parametrizing microphysical processes in the jet and vortex phase on contrail cirrus properties and radiative forcing. *J. Geophys. Res. Atmos.* **127**, e2022JD036677. https://doi.org/10.1029/2022JD036677 (2022).

54. Zhang, W. et al. Impact of host climate model on contrail cirrus effective radiative forcing estimates. *Atmos. Chem. Phys.* **25**, 473–489, https://doi.org/10.5194/acp-25-473-2025 (2025).

55. Rubin-Zuzic, M., Bugliaro, L. G., Marsing, A. et al. Reduced contrail radiative effect for future fleets with low soot and water vapour emissions. *Atmospheric Environment: X*. **27**, 100353, https://doi.org/10.1016/j.aeaoa.2025.100353 (2025).

56. Gasser, T., Ciais, P., Boucher, O. *et al.* The compact Earth system model OSCAR v2.2: description and first results. *Geosci. Model Dev.* **10**, 271–319, https://doi.org/10.5194/gmd-10-271-2017 (2017).

57. ICCT. Aviation Vision 2050: The potential for climate-neutral growth, ID-445-–-Aviation-Vision-2050_report_final-2.pdf (2025).

741 58. ICAO. Jointly regulating jet fuel aromatic and sulfur content: A near-term strategy for public health and climate
742 benefits, https://www.icao.int/sites/default/files/sp-files/environmental-protection/Documents/EnvironmentReport-
743 2010/2025/Envreport2025_101.pdf (2025).

744 59. Bickel, M., Ponater, M., Burkhardt, U. et al. Contrail Cirrus Climate Impact: From Radiative Forcing to Surface
745 Temperature Change. *J Clim.* **38**, 1895–1912, https://doi.org/10.1175/JCLI-D-24-0245.1 (2025).

746 60. Rap, A., Forster, P. M., Haywood, J. M. et al. Estimating the climate impact of linear contrails using the UK Met
747 Office climate model. *Geophys. Res. Lett.* **37**, L20703, https://doi.org/10.1029/2010GL045161 (2010).

748 61. Ponater, M. Distinctive efficacies of the components con tributing to total aviation climate impact. Proc. Second
749 Int. Conf. on Transport, Atmosphere and Climate (TAC–2), Aachen, Germany, Deutsches Zentrum für Luft- und
750 Raumfahrt, 227-232, https://elib.dlr.de/65284/ (2010).

751 62. Joos, F., Roth, R., Fuglestvedt, J. S. et al. Carbon dioxide and climate impulse response functions for the
752 computation of greenhouse gas metrics: a multi-model analysis. *Atmos. Chem. Phys.* **13**, 2793–2825,
753 https://doi.org/10.5194/acp-13-2793-2013 (2013).

754 63. Megill, L., Deck, K. & Grewe, V. Alternative climate metrics to the Global Warming Potential are more suitable
755 for assessing aviation non-CO2 effects. *Commun Earth Environ* **5**, 249, https://doi.org/10.1038/s43247-024-01423-6
756 (2024).

757 64. Shine, K. P., Derwent, R. G., Wuebbles, D. J. et al. in Climate Change: The IPCC Scientific Assessment by
758 Working Group 1 (eds Houghton J. T. et al.) Ch. 2 (Cambridge Univ. Press) (1990).

759 65. Allen, M.R., Peters, G.P., Shine, K.P. *et al.* Indicate separate contributions of long-lived and short-lived greenhouse
760 gases in emission targets. *npj Clim Atmos Sci* **5**, 5, https://doi.org/10.1038/s41612-021-00226-2 (2022).

761 66. Prather, M.J., Gettelman, A. & Penner, J.E. Trade-offs in aviation impacts on climate favour non-
762 CO_2 mitigation. *Nature* **643**, 988–993, https://doi.org/10.1038/s41586-025-09198-2 (2025).

763 67. ICAO. LTAG data spreadsheet, https://www.icao.int/LTAG-data-spreadsheet (2022).

764 68. Schumann, U. & Seifert, A. On the Weather Impact of Contrails: New Insights from Coupled ICON–CoCiP
765 Simulations, *Atmos. Chem. Phys.* **25**, 18571–18597, https://doi.org/10.5194/acp-25-18571-2025 (2025).

766 69. Bräuer, T., Voigt, C., Sauer, D. et al. Airborne measurements of contrail ice properties—Dependence on
767 temperature and humidity. *Geophys. Res. Lett.* **48**, e2020GL092166, https://doi.org/10.1029/2020GL092166 (2021).

768 70. Ponsonby, J., Teoh, R., Kärcher, B. et al. An updated microphysical model for particle activation in contrails: the
769 role of volatile plume particles. *Atmos. Chem. Phys.* **25**, 18617–18637, https://doi.org/10.5194/acp-25-18617-2025
770 (2025).

771 71. Ungeheuer, F., Caudillo, L., Ditas, F. et al. Nucleation of jet engine oil vapours is a large source of aviation-related
772 ultrafine particles. *Commun Earth Environ* **3**, 1, https://doi.org/10.1038/s43247-022-00653-w (2022).

72. Neumann, G., Marsing, A., Harlass, T. et al. In-flight emission measurements with an autonomous payload behind a turboprop aircraft. *Atmos. Meas. Tech.* **18**, 6795–6816, https://doi.org/10.5194/amt-18-6795-2025 (2025).77. ATAG. Briefing: SAF scale-up through regulation. ECAC Environment Forum / 7, Paris, 29 May 2024.

73. Shapiro, M., Engberg, Z., Teoh, R. et al. pycontrails: Python library for modeling aviation climate impacts, Zenodo (code), https://doi.org/10.5281/zenodo.7776686 (2023).

74. Emde, C., Buras-Schnell, R., Kylling, A. et al. The libRadtran software package for radiative transfer calculations (version 2.0.1). *Geosci. Model Dev.* **9**, 1647–1672, https://doi.org/10.5194/gmd-9-1647-2016 (2016).

75. Jurkat-Witschas, T., Voigt, C., Groß, S. et al. CIRRUS-HL: Picturing high- and mid-latitude summer cirrus and contrail cirrus above Europe with airborne measurements aboard the research aircraft HALO. *Bull. Amer. Meteor. Soc*. https://doi.org/10.1175/BAMS-D-23-0270.1 (2025).

76. Schumann, U., Baumann, R., Baumgardner, D. et al. Properties of individual contrails: a compilation of observations and some comparisons. *Atmos. Chem. Phys.* **17**, 403–438, https://doi.org/10.5194/acp-17-403-2017 (2017).

77. Dannet, G., Boucher, O, & Bellouin, N. Features and evolution of civil aviation CO_2 emissions based on ADS-B data for the period between 2019–2024. *Metascience in Aerospace*, **1**(4), 346-370, https://doi.org/10.3934/mina.2024016 (2024).

78. WMO. WMO report, https://wmo.int/files/state-of-climate-update-cop30 (2025).

79. EU. Horizon project JETSCREEN. Deliverable D7.3 Report and analysis of APU emission measurements. https://cordis.europa.eu/project/id/723525/results (2020).

Supplementary Files

This is a list of supplementary files associated with this preprint. Click to download.

- Usingaviationfuelhydrogencontenttoassesscontrailsandclimateimpactsupplementary20260804.pdf